Acta Crystallographica Section B
Structural Science
ISSN 0108-7681

Triclinic apatites

Tom Baikie,[a]* Patrick H. J. Mercier,[b] Margaret M. Elcombe,[c] Jean Y. Kim,[a] Yvon Le Page,[b] Lyndon D. Mitchell,[d] T. J. White[a] and Pamela S. Whitfield[b]

[a]School of Materials Science and Engineering, Nanyang Technological University, Block N4.1, Nanyang Avenue, Singapore 639798, [b]Institute for Chemical Process and Environmental Technology, National Research Council of Canada, 1200 Montreal Road, Ottawa, Canada K1A 0R6, [c]The Bragg Institute, Australian Nuclear Science and Technology Organisation, PMB 1, Menai NSW 2234, Australia, and [d]Institute for Research in Construction, National Research Council of Canada, 1200 Montreal Road, Ottawa, Canada K1A 0R6

Correspondence e-mail: tbaikie@ntu.edu.sg

Received 21 November 2006
Accepted 8 December 2006

Apatites commonly adopt $P6_3/m$ hexagonal symmetry. More rarely, monoclinic chemical analogues have been recognized, including the biologically significant hydroxyapatite, $Ca_{10}(PO_4)_6(OH)_2$, but the driving force towards lower symmetry has not been systematically examined. A combination of diffraction observations and *ab initio* calculations for $Ca_{10}(AsO_4)_6F_2$ and $Ca_{10}(VO_4)_6F_2$ show these materials are triclinic $P\bar{1}$ apatites in which the AsO_4 and VO_4 tetrahedra tilt to relieve stress at the metal and metalloid sites to yield reasonable bond-valence sums. An analysis of the triclinic non-stoichiometric apatites $La_{10-x}(GeO_4)_6O_{3-1.5x}$ and $Ca_{10}(PO_4)_6(OH)_{2-x}O_{x/2}$ confirms this scheme of tetrahedral rotations, while $Cd_{10}(PO_4)_6F_2$ and $Ca_{10}(CrO_4)_6F_2$ are predicted to be isostructural. These distortions are in contrast to the better known $P112_1/b$ monoclinic dimorphs of chloroapatite and hydroxyapatite, where the impetus for symmetry reduction is ordered anion (OH^- and Cl^-) displacements which are necessary to obtain acceptable bond lengths. These results are important for designing apatites with specific structural and crystal-chemical characteristics.

1. Introduction

Hydroxyapatite is a familiar biomaterial for bone replacement (Weiner & Wagner, 1998) and the apatite crystal family is of considerable importance in environmental remediation (Manecki *et al.*, 2000) and catalysis (Eon *et al.*, 2006), and as fertilisers (Bolland *et al.*, 1995), electrolytes (Nakayama *et al.*, 1995) and phosphors (Li *et al.*, 2006). The structure of apatites, whose general formula can be written as $A^{I}_4A^{II}_6(BO_4)_6X_2$ (A = large cations; B = metalloids; X = anion and oxyanions) accommodates diverse chemistries with more than 74 discrete varieties now recognized (White *et al.*, 2005). These disparate compositions are possible because of the inherent flexibility of an $A^{I}_4(BO_4)_6$ framework that circumscribes one-dimensional tunnels, which expand or contract in response to the filling characteristics of the $A^{II}_6X_2$ component (White & Dong, 2003). While the default symmetry for apatites is hexagonal $P6_3/m$ only 57% of chemical end-members adopt this space group; a further 34% crystallize in hexagonal subgroups ($P6_3$, $P\bar{6}$ and $P\bar{3}$), with the balance monoclinic (White *et al.*, 2005). Recently, two $P\bar{1}$ apatites [$La_{10-x}(GeO_4)_6O_{3-1.5x}$, $9.66 < 10 - x < 9.75$ (León-Reina *et al.*, 2003; Abram *et al.*, 2005) and $Ca_{10}(PO_4)_6(OH)_{2-x}O_{x/2}$ ($0.78 < x < 1.56$); Alberius-Henning *et al.*, 2001] have been reported, but no general conclusions concerning the origin of the triclinic distortions were drawn.

Although details pertaining to lower-symmetry apatites are sparse, their existence has long been recognized (Organova *et al.*, 1994; Kriedler & Hummel, 1970; Banks & Jauanarajs, 1965). In an early stability field diagram, Kreidler & Hummel

(1970) showed that the metal-substituted fluoroapatites $Ca_{10}(AsO_4)_6F_2$, $Ca_{10}(VO_4)_6F_2$ and $Cd_{10}(PO_4)_6F_2$ were distorted, as the ionic radius of the *B*-type metalloid was large relative to the *A* cation. Banks & Jauanarajs (1965) observed a similar structural distortion in $Ca_{10}(CrO_4)_6F_2$. However, a rigorous examination of the modifications accompanying apatite symmetry changes has not been attempted because the structure is inherently difficult to visualize and an undistorted prototype, against which structural adjustments can be calibrated, did not exist. In a re-examination of this problem, we have shown (White *et al.*, 2005; White & Dong, 2003) that apatites can be simply described as zeolite-like microporous frameworks composed of face-sharing $A^{\rm I}O_6$ trigonal prismatic columns that are corner-connected to the BO_4 tetrahedra (Fig. 1). The channels can adjust their size to suit the remaining $A^{\rm II}_6X_2$ by converting the trigonal prisms to metaprisms through rotation of the triangular faces over an angle φ. In practice, $5 \leq \varphi \leq 25^\circ$ and the smaller the $A^{\rm II}_6X_2$ portion relative to the $A^{\rm I}_4(BO_4)_6$ framework, the larger the metaprism twist angle. From the trigonal prismatic prototype, a geometrical parameterization of $P6_3/m$ apatites has been developed that allows structural refinement from crystal chemical parameters in which polyhedral distortions conform to *ab initio* minimum-energy solutions for apatites of different compositions (Mercier *et al.*, 2005, 2006, 2007). To assess the distortions of metal-substituted fluoroapatites, an experimental and theoretical investigation was launched to examine the crystal structures of $Ca_{10}(AsO_4)_6F_2$ and $Ca_{10}(VO_4)_6F_2$. In this report, electron, neutron and X-ray powder diffraction as well as *ab initio* calculations were used to show that these compounds are isostructural triclinic $P\bar{1}$ apatites and that the reduction of symmetry from $P6_3/m$ is caused by BO_4 tetrahedral tilting to obtain satisfactory bond-valence sums.

2. Experimental methods

$Ca_{10}(AsO_4)_6F_2$ and $Ca_{10}(VO_4)_6F_2$ were synthesized in the solid-state through reaction of CaO (obtained by firing AR grade $CaCO_3$ at 1173 K), As_2O_3, V_2O_5 and CaF_2 mixed in stoichiometric proportions at 1073 K for 15 h. Grinding and re-firing were repeated until a single-phase product was obtained.

Neutron powder diffraction data were collected on the high-resolution powder diffractometer (HRPD) at the High Flux Australian Reactor (HIFAR) operated by the Australian Nuclear Science and Technology Organization (ANSTO). A neutron wavelength of 1.8845 Å was used from 0.029 to 150.079° 2θ in 0.05° steps. Approximately 15 g of each apatite was loaded into a 12 mm diameter vanadium can that was rotated during data collection. Structure refinement was carried out from 10 to 150° 2θ using the software *TOPAS*, Version 3.0 (Bruker, 2005). A pseudo-Voigt peak shape corrected for asymmetry was used. The refined instrument parameters included four polynomial background coefficients, peak half widths *U*, *V*, *W* and an asymmetry parameter. The scattering lengths 0.470, 0.6580, 0.5805 and 0.5654 $\times 10^{-12}$ cm were used for Ca, As, O and F, respectively. As vanadium is transparent to neutrons (-0.0443×10^{-12} cm), its coordinates were determined *via* X-ray powder diffraction.

X-ray powder data were collected with a Shimadzu LabX XRD-6000 diffractometer (Bragg–Brentano geometry) equipped with a Cu $K\alpha$ X-ray tube operated at 40 kV and 40 mA. Samples were mounted in a top-loaded trough, which was not rotated during data collection. Under these conditions, the intensity of the strongest peak was 10 000–12 000 counts. Rietveld refinement of X-ray data was performed using the fundamental-parameters approach and a full axial divergence model (Cheary & Coelho, 1992, 1998). Refined specimen-dependent parameters included the zero error, a user-specified number of coefficients of a Chebyshev polynomial fitting the background and the 'crystallite size'.

Selected-area electron diffraction patterns (SAED) were collected from powders ultrasonically dispersed in ethanol with several drops of suspension deposited onto a holey carbon-coated copper grid. A Jeol-2100 microscope operating at 200 kV and fitted with a double-tilt holder was used to locate the required orientations.

The modelling and *ab initio* interface software environment *Materials Toolkit*, Version 2.0 (Le Page & Rodgers, 2005), was used to prepare input files for *ab initio* total-energy minimization calculations with *VASP*4.6.3 (Kresse, 1993; Kresse & Hafner, 1993, 1994). The common execution parameters were: GGA PAW potentials (Kresse & Joubert, 1999); electronic convergence at 1×10^{-7} eV, convergence for forces of 1×10^{-4} eV Å^{-1}; Davidson-blocked iterative optimization of the wavefunction in combination with reciprocal-space projectors (Davidson, 1983); a Methfessel–Paxton (Methfessel & Paxton, 1999) smearing scheme of order 1 and width 0.2 eV

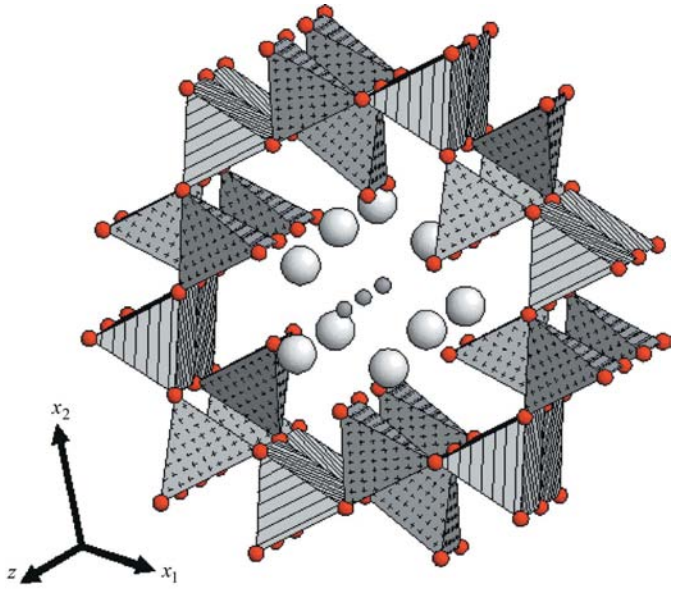

Figure 1
Apatite prototype structure in which $A^{\rm I}O_6$ trigonal prisms share faces along [001] and are corner-connected to BO_4 tetrahedra to form one-dimensional channels that are filled by $A^{\rm II}$ and *X* ions.

Table 1
Tetrahedral tilt angles for $P\bar{1}$ apatites.

The calculations for the tetrahedral tilt angles were performed as follows: Cartesian coordinates in the IRE reference system (IRE standard; Brainerd, 1949) were first obtained for all the appropriate O atom sites. As the Z axis of the IRE reference system points along the triclinic c vector, the values of the rotation or tilt angles could then be easily extracted from the corresponding Cartesian coordinates of the O atoms.

Tetrahedra	Along a (°)	Along b (°)	Along [110] (°)
As-AP	12	11	5
V-AP	8.5	9.5	3
Oxy-HAP[(a)]	14	6	1
$La_{10-x}(GeO_4)_6O_{3-1.5x}$[(b)]	18.5	13.5	3

References: (*a*) Alberius-Henning *et al.*, 2001); (*b*) León-Reina *et al.* (2003).

for energy corrections; a k-mesh dimension of $2 \times 2 \times 3$ for reciprocal space integration (Monkhorst & Pack, 1976). Spin polarization corrections were not used. The calculations took about 5 d per triclinic structure on a single 3 GHz Athlon-64 PC running *VASP*4.6.3 under Microsoft® Windows® using the execution scheme described above.

Secondary electron images (SEI) were collected using a Hitachi S-4800 Field Emission Scanning Electron Microscope. The instrument was fitted with two secondary detectors and composite images acquired at a working distance of 8 mm using a beam energy of 2 kV and 5 μA current. Typical SEI of $Ca_{10}(AsO_4)_6F_2$ and $Ca_{10}(VO_4)_6F_2$ confirmed the samples to be crystalline and homogeneous (see Figs. S1*a* and S1*b* of the supplementary data[1]). An Oxford Inca EDS (energy-dispersive spectroscopy) system provided semi-quantitative elemental analyses consistent with the expected metal proportions.

3. Results and discussion

For $Ca_{10}(AsO_4)_6F_2$ the a^* and c^* vectors in [010] selected-area electron diffraction patterns are clearly not orthogonal because the reciprocal lattice vectors from the reflection $\bar{3}0\bar{2}^*$ to 302^* are relatively shorter by $\sim 1.5\%$ compared with $\bar{3}02^*$ to $30\bar{2}^*$ (Fig. 2*a*). This precludes the existence of a symmetry axis along **c** and a symmetry plane perpendicular to it, which proves the material to be triclinic ($P\bar{1}$ or $P1$). In addition, the patterns show no superlattice reflections, which confirms the triclinic distortion is fundamentally different from the monoclinic type previously described in chloroapatite (Mackie *et al.*, 1972; Bauer & Klee, 1993) and hydroxyapatite (Elliott *et al.*, 1973; Suetsugu & Tanaka, 2002) where a doubling of the b axis is characteristic.

Starting from the approximate cell constants obtained by electron diffraction and a $P\bar{1}$ structural model using fractional coordinates adapted from fluoroapatite (Sudarsanan *et al.*, 1972), a satisfactory profile fit (Fig. S2*a* of the supplementary material), accurate unit-cell parameters and refined atomic positions could be extracted from the neutron diffraction profile by Rietveld refinement (see Table S1*a* of the supplementary material). Selected bond lengths are given in Table S2 of the supplementary material. Similar structural refinements in space groups $P6_3/m$ and $P112_1/m$ yielded agreement factors (R_{wp} and R_{Bragg} values) that were of inferior quality to those obtained using $P\bar{1}$ (see Fig. S2*a* and Table S3 of the supplementary material). *Ab initio* optimization of cell constants and atomic coordinates of $Ca_{10}(AsO_4)_6F_2$ through total energy minimization was performed assuming $P6_3/m$ and $P\bar{1}$ symmetry. The lower energy of the triclinic model over the hexagonal one is consistent with the observed stability of the former and yields cell edges and angles together with fractional coordinates (Table S4) close to the refined values (Table S1*a*). Those results argue strongly in favour of the correctness of the $P\bar{1}$ triclinic structure for $Ca_{10}(AsO_4)_6F_2$.

The non-perpendicularity of a^* and c^* is less obvious for $Ca_{10}(VO_4)_6F_2$ (Fig. 2) because the departure from the hexagonal metric is about half that of the arsenic material, but the vector $\bar{3}02^*$ is perceptibly longer than 302^*. Cell data and composite structure results with Ca and O fractional coordinates from neutron diffraction and V positions from X-ray diffraction are shown in Table S1*b* and Fig. S2(*b*) of the supplementary material. Overall, these hybrid results for $Ca_{10}(VO_4)_6F_2$ are not as precise as those for $Ca_{10}(AsO_4)_6F_2$ and lead to approximate but not entirely convincing BVS (bond-valence sums). However, a superior triclinic structural model (Table S5 of the supplementary material) was built from the experimental coordinates for $Ca_{10}(AsO_4)_6F_2$ (Table S1*a*) and the cell data of Dong & White (2004) for the proposed monoclinic structure of $Ca_{10}(VO_4)_6F_2$. Here the oxygen coordinates were adjusted to allow for a 2% expansion of V—O bond lengths with respect to As—O bond lengths, with no change in the cation positions, rotations and bond angles of the BO_4 tetrahedra. This procedure gave average BVS of 1.972, 1.946 and 5.022 v.u. (valence units) for the $A^{\rm I}$, $A^{\rm II}$ and B sites, respectively. This is a considerable improvement over the BVS from Mercier *et al.* (2007) for hexagonal $Ca_{10}(V_xP_{1-x}O_4)_6F_2$ structures with compositions close to the V end-member, as well as the BVS calculated using the monoclinic structure of $Ca_{10}(VO_4)_6F_2$ (V-AP) reported in Dong & White (2004). The changes with respect to the experimental input atom coordinates that were observed upon *ab initio* optimization of this triclinic model were small and the cell angles agree with the refined cell data within 0.17° (Tables S6 with S5 of the supplementary material). The similarity of the axial ratios and angles (a/b, c/b, α, β, γ), and the corresponding atom positions between experimental (Table S1*a*) and *ab initio* (Table S6) results for $Ca_{10}(VO_4)_6F_2$ compared with neutron (Table S1*a*) and *ab initio* (Table S4) results for $Ca_{10}(AsO_4)_6F_2$ confirms that these apatites have similar geometrical configurations, *i.e.* similar bond angles and polyhedral rotations.

$Ca_{10}(PO_4)_6F_2$ (F-AP) (Fig. 3*a*) and $Ca_{10}(AsO_4)_6F_2$ (As-AP; Fig. 3*b*) differ primarily in the rotations of the symmetry-independent tetrahedra in the triclinic As-AP (Table 1). Two pairs of tetrahedra directed along a and b rotate by similar

[1] Supplementary data for this paper are available from the IUCr electronic archives (Reference: LM5005). Services for accessing these data are described at the back of the journal.

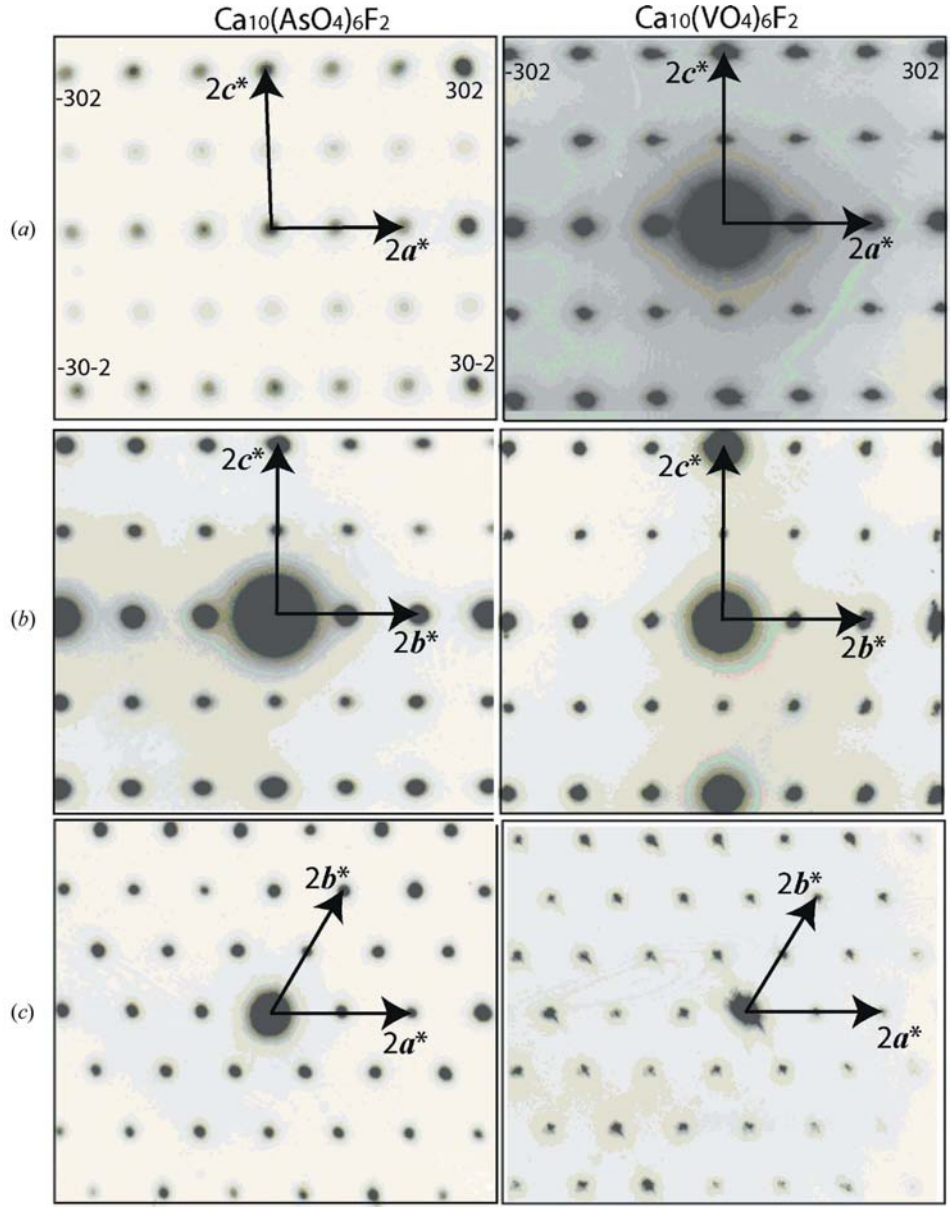

Figure 2
Selected-area electron diffraction patterns of $Ca_{10}(AsO_4)_6F_2$ and $Ca_{10}(VO_4)_6F_2$: (*a*) [010], (*b*) [100] and (*c*) [001].

angles of 12 and 11°, respectively, about the normal to one of their faces that was perpendicular to the (001) mirror in F-AP. The third pair of tetrahedra along [110] tilt by a modest 5° about their edges that lie on the mirror plane in F-AP (Table 1). Similar analyses of V-AP, oxy-hydroxyapatite (oxy-HAP; Alberius-Henning *et al.*, 2001; Fig. 3*c*) with a 78% degree of dehydration, and triclinic $La_{10-x}(GeO_4)_6O_{3-1.5x}$ (León-Reina *et al.*, 2003; Table 1), revealed the same tetrahedral tilting scheme confirming that the materials are isostructural. While *ab initio* modelling of the latter non-stoichiometric materials is not possible, calculations for $Ca_{10}(PO_4)_6O$ (Table S7) and $La_{10}(GeO_4)_6O_3$ (Table S8), yield cell parameters and structural distortions not far removed from the experimental results for non-stoichiometric, stable materials.

In a separate study of the $Ca_{10}(V_xP_{1-x}O_4)_6F_2$ compounds (Mercier *et al.*, 2007), the origin of the symmetry reduction in the end-member $Ca_{10}(VO_4)_6F_2$ is clear: if $P6_3/m$ symmetry is retained, the BVS at the A^{II} calcium site decreases linearly with increasing vanadium content, with a large increase in BVS at the tetrahedral site as the phase transition is approached. Crystal chemical analysis shows that the combination of a small divalent cation at the *A* sites and a large pentavalent metalloid at the *B* site leads to extension stress at A^{II} (BVS < +2 v.u.) and compressive stress at *B* (BVS > +5 v.u.). As V^{5+} and As^{5+} are both large tetrahedral pentavalent ions, it is concluded that the symmetry reduction in $Ca_{10}(AsO_4)_6F_2$ is also driven by the need to reduce considerable over-bonding at *B*. Bond-valence sums for calcium and arsenic sites for the refined triclinic phase show much-relieved stress with average values of 1.989, 1.949 and 5.124 v.u. at the putative A^I, A^{II} and *B* sites, respectively. This is well within BVS variability commonly observed in minerals and inorganic compounds (Brown & Altermatt, 1985).

Tetrahedral rotations seen in Figs. 3(*b*) and (*c*) achieve precisely the bond-valence regularization described above. The larger size of vanadium and arsenic with respect to phosphorus increases the distance between A^I metaprisms and enlarges the tunnel diameter. This leads to a gradual under-bonding at the Ca^{II} positions and over-bonding at the *B* positions upon the addition of larger metalloids. In $P6_3/m$ the VO_4/AsO_4 tetrahedra are constrained to rotate around an axis parallel to *c* that further separates the A^IO_6 metaprisms in the *ab* plane increasing the diameter of the pores, and leads to a severe under-bonding of the Ca^{II} ions. This dilemma is overcome by lowering the symmetry. By removing a mirror plane, tetrahedra are free to rotate around an axis perpendicular to *c*, such that one O of the BO_4 unit moves towards Ca^{II} while another more strongly caps the Ca^I prism faces. This structural adjustment simultaneously results in a more acceptable BVS for the A^I and A^{II} sites, whilst establishing pentavalence at *B*. Using similar arguments

together with quantum mechanical energy minimization, it is predicted that the distorted apatites $Cd_{10}(PO_4)_6F_2$ (Kreidler & Hummel, 1970; Table S9) and $Ca_{10}(CrO_4)_6F_2$ (Banks & Jauanarajs, 1965; Table S10) will also adopt $P\bar{1}$ symmetry.

Le Page & Rodgers (2005) attribute symmetry reduction in chloroapatite to the Cl atoms, on the basis that all other atoms conform to $P6_3/m$ symmetry within 0.16 Å while the halide coordinates deviate by 0.43 Å. When chloro- and fluoroapatites are compared it is found that chlorine, being larger than fluorine, would have a BVS exceeding −1 v.u., if it was located at the $\bar{6}$ position on the mirror plane containing the Ca^{II} atoms to which it is bonded. Consequently, Cl ions alternately occupy positions above and below the mirror plane, with inter-tunnel correlation along the *b* axis, transforming this mirror into a *b*-glide plane. This lowers the symmetry to monoclinic $P112_1/b$, doubles the *b* axis and causes slight tilting of BO_4 tetrahedra (Fig. S3*a*). Analysis of monoclinic hydroxyapatite (Elliott *et al.*, 1973; Suetsugu & Tanaka, 2002) shows very similar structural adjustments (Fig S3*b*). Rather than adopting the $P6_3$ isomorphic subgroup of $P6_3/m$ that would accommodate ordered hydroxyl in a hexagonal space group, OH groups are seen to alternate above and below the Ca–Ca–Ca triangular units, which leads to displacements of the A^{II} ions away from the mirror plane in $P6_3/m$ and results in a tilting of the tetrahedra to accommodate these displacements. While the symmetry reduction to monoclinic in chloroapatite and hydroxyapatite is caused by ordered anion displacements to achieve chemically correct BVS at the anion (*X*) sites in the tunnels, the triclinic structures of the calcium arsenate and vanadate apatite arise to relieve stresses at metal (*A*) and metalloid (*B*) sites caused by the larger size of the $A^{I}_4(BO_4)_6$ framework relative to the $A^{II}_6X_2$ component.

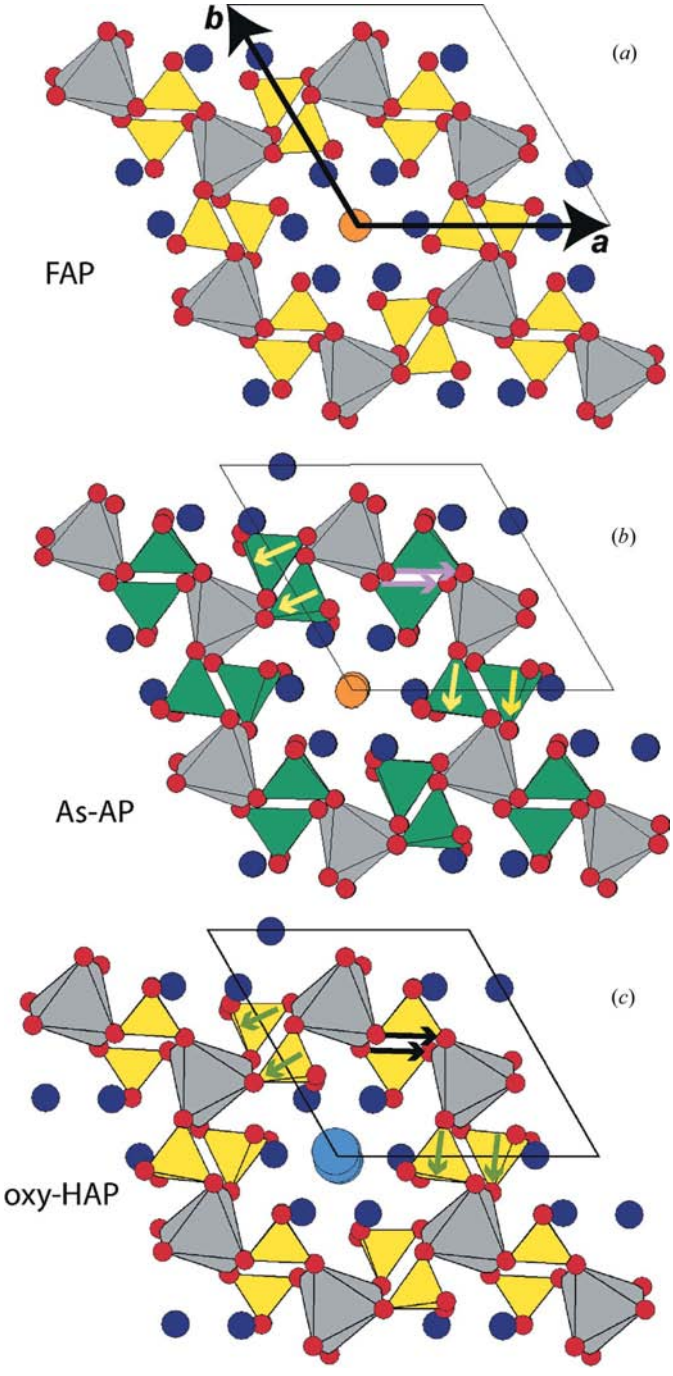

Figure 3
Polyhedral representation of (*a*) $Ca_{10}(PO_4)_6F_2$, in which there is no tilting of the tetrahedra, (*b*) $Ca_{10}(AsO_4)_6F_2$ and (*c*) $Ca_{10}(PO_4)_6(OH)_{2-x}O_{x/2}$ with $x = 1.56$, where the tetrahedra directed along *a*, *b* and [110] rotate about axes as indicated by the arrows. Unlike the prototype (Fig. 1), the trigonal prisms have twisted their triangular faces to create metaprisms, which are polyhedra midway between trigonal prisms and octahedra.

4. Conclusions

In summary, electron diffraction has demonstrated that $Ca_{10}(AsO_4)_6F_2$ and $Ca_{10}(VO_4)_6F_2$ are the first reported examples of stoichiometric triclinic apatites. Neutron and X-ray diffraction substantiate this analysis and show that the rotation of the BO_4 tetrahedra lowers the symmetry from $P6_3/m$ to $P\bar{1}$, while preserving topology and achieving more satisfactory BVS. *Ab initio* calculations provide further confirmation that the $P\bar{1}$ structure is energetically favoured, reproduces the unit-cell distortions and provides optimized atomic coordinates close to the observed values. This distortion is required when the $A^{I}_4(BO_4)_6$ framework is expanded with respect to the $A^{II}_6X_2$ channel contents. The origin of triclinic $P\bar{1}$ symmetry is distinct from the phase change to $P112_1/b$ monoclinic in hydroxy- and chloroapatite where the tunnel/channel framework nearly retains $P6_3/m$ symmetry, but is penetrated by an ordered arrangement of the *X* anions that cause A^{II} cationic displacements along *c* accompanied by slight tetrahedral tilting, leading to a non-maximal subgroup of the $P6_3/m$ parent. The ability to model the crystallographic distortions of apatites is of fundamental importance for tailoring chemical analogues with specific chemical and physical functionality.

This work was supported through a joint NRC-A*STAR research program on 'Advanced Ceramic Methods for the Co-stabilization and Recycling of Incinerator Fly Ash with Industrial Wastes'. The authors would like to thank Dr Wim Klooster for collecting the neutron diffraction data and Jim

Margeson for scanning electron microscopy and energy-dispersive X-ray spectroscopy analyses. In addition, the authors gratefully acknowledge the informal reviews and detailed comments provided by Professors Giovanni Ferraris and Jim Elliott.

References

Abram, A. J., Kirk, C. A., Sinclair, D. C. & West, A. J. (2005). *Solid State Ion.* **176**, 1941–1947.

Alberius-Henning, P., Adolfson, E., Grins, J. & Fitch, A. (2001). *J. Mater. Sci.* **36**, 663–668.

Banks, E. & Jauanarajs, K. L. (1965). *Inorg. Chem.* **4**, 78–83.

Bauer, M. & Klee, W. E. (1993). *Z. Kristallogr.* **206**, 15–24.

Bolland, M. D. A., Clarke, M. F. & Yeates, J. S. (1995). *Fertilizer Res.* **41**, 129–143.

Brainerd, J. G. *et al.* (1949). *Proc. Inst. Radio Eng.* **37**, 1378–1949. (Reprinted from IRE standard, 1949 IRE 14.S1.)

Brown, I. D. & Altermatt, D. (1985). *Acta Cryst.* B**41**, 244–247.

Bruker (2005). *Topas*, Version 3.0. Bruker AXS, Karlsruhe, Germany.

Cheary, R. W. & Coelho, A. (1992). *J. Appl. Cryst.* **25**, 109–121.

Cheary, R. W. & Coelho, A. (1998). *J. Appl. Cryst.* **31**, 851–861.

Davidson, E. R. (1983). *NATO Advanced Study Institute Series C*, edited by G. H. F. Diercksen & S. Wilson, Vol. 113, p. 95. New York: Plenum Press.

Dong, Z. & White, T. J. (2004). *Acta Cryst.* B**60**, 146–154.

Elliott, J. C., Mackie, P. E. & Young, R. A. (1973). *Science*, **180**, 1055–1057.

Eon, J. G., Boechat, C. B., Rossi, A. M., Terra, J. & Ellis, D. E. (2006). *Phys. Chem. Chem. Phys.* **8**, 1845–1851.

Kresse, G. (1993). PhD thesis. Technische Universität Wien, Austria.

Kresse, G. & Hafner, J. (1993). *Phys. Rev. B*, **48**, 13115–13118.

Kresse, G. & Hafner, J. (1994). *Phys. Rev. B*, **49**, 14251–14269.

Kresse, G. & Joubert, J. (1999). *Phys. Rev. B*, **59**, 1758–1775.

Kriedler, E. R. & Hummel, F. A. (1970). *Am. Mineral* **55**, 170–184.

Le Page, Y. & Rodgers, J. (2005). *J. Appl. Cryst.* **38**, 697–705.

León-Reina, L., Martin-Sedeño, M. C., Losilla, E. R., Cabeza, A., Martinez-Lara, M., Bruque, S., Marques, F. M. B., Sheptyakov, D. V. & Aranada, M. A. G. (2003). *Chem. Mater.* **15**, 2099–2108.

Li, Y. C., Chang, Y. H., Tsai, B. S., Chen, Y. C. & Lin, Y. F. (2006). *J. Alloys Comp.* **416**, 199–205.

Mackie, P. E., Elliott, J. C. & Young, R. A. (1972). *Acta Cryst.* B**28**, 1840–1848.

Manecki, M., Maurice, P. A. & Traina, S. J. (2000). *Am. Mineral.* **85**, 932–943.

Mercier, P. H. J., Le Page, Y., Whitfield, P. S., Mitchell, L. D., Davidson, I. J. & White, T. J. (2005). *Acta Cryst.* B**61**, 635–655.

Mercier, P. H. J., Le Page, Y., Whitfield, P. S. & Mitchell, L. D. (2006). *J. Appl. Cryst.* **39**, 369–375.

Mercier, P. H. J., Dong, Z., Baikie, T., Le Page, Y., White, T. J., Whitfield, P. S. & Mitchell, L. D. (2007). *Acta Cryst.* B**63**, 37–48.

Methfessel, M. & Paxton, A. T. (1999). *Phys. Rev. B*, **40**, 3616–3621.

Monkhorst, H. J. & Pack, J. D. (1976). *Phys. Rev. B*, **13**, 5188–5192.

Nakayama, S., Aono, H. & Sadaoka, Y. (1995). *Chem. Lett.* **24**, 431–432.

Organova, N. I., Rastsvetaeva, R. K., Kuz'mina, O. V., Arapova, G. A., Litsarev, M. A. & Fin'ko, V. I. (1994). *Kristallografiya*, **39**, 278–282.

Suetsugu, Y. & Tanaka, J. (2002). *J. Mater. Sci. Mater. Med.* **13**, 767–772.

Sudarsanan, K., Mackie, P. E. & Young, R. A. (1972). *Mater. Res. Bull.* **7**, 1331–1338.

Weiner, S. & Wagner, H. D. (1998). *Ann. Rev. Mater. Sci.* **228**, 271–298.

White, T. J. & Dong, Z. (2003). *Acta Cryst.* B**59**, 1–16.

White, T. J., Ferraris, C., Kim, J. & Madhavi, S. (2005). *Rev. Miner. Geochem.* **57**, 307–401.